CPC(HEP & NP), 2009, **33**(Suppl.Ⅱ): 65—70 **Chinese Physics C** Vol. 33, Suppl.Ⅱ, Jun., 2009

Beam dynamics studies on BEPC-Ⅱ storage rings at the commissioning stage*

QIN Qing(秦庆)[1)] HUANG Nan(黄楠) LIU Wei-Bin(刘渭滨) LIU Yu-Dong(刘瑜冬)
PENG Yue-Mei(彭月梅) QIU Jing(邱静) WANG Dou(王逗) WANG Xin-Hao(王昕昊)
WANG Na(王娜) WANG Jiu-Qing(王九庆) WEI Yuan-Yuan(魏源源) WEN Xue-Mei(温雪梅)
XING Jun(邢军) XU Gang(徐刚) YU Cheng-Hui(于程辉) ZHANG Chuang(张闯)
ZHANG Yuan(张源) ZHAO Zheng(赵政) ZHOU De-Min(周德民)

(Institute of High Energy Physics, Chinese Academy of Sciences, Beijing 100049, China)

Abstract During the 1st and 2nd stages of the commissioning of the upgrade project of the Beijing Electron Positron Collider (BEPCⅡ), which started on Nov. 12, 2006 and Oct. 24, 2007, respectively, we got the luminosity one tenth of its design value, provided beams to synchrotron radiation users for about 4 months, and studied beam dynamics as well. In this paper, some beam dynamics studies on the storage rings and their preliminary results are given.

Key words BEPCⅡ, commissioning, beam dynamics, luminosity

PACS 29.27.Bd, 29.20.db

1 Introduction

The BEPCⅡ is composed of a linac, two transport lines and three storage rings. Among them, two rings are in parallel for e- and e+ beams, respectively, and the two halves of the outer rings are connected as a synchrotron radiation (SR) ring, with 14 beam lines extracted from 5 wigglers and 9 bending magnets. The layout and other details of the three rings of BEPCⅡ can be found in Ref. [1].

In this paper, we discuss some beam dynamics studies carried out in three rings, BER and BPR for e- and e+ beams, respectively, and BPR for SR. Some design parameters of the two lattices, collision and dedicated SR, are listed in Tables 1 and 2.

Both BER and BPR have the same magnetic lattices with the super-period number of 1. Fig. 1 shows the Twiss functions in the interaction region, the RF region and the whole BER/BPR rings. In order to have a big emittance and a high beam current for collision, a quasi-FODO structure with 10 dipoles and 2 missing dipoles in each arc is applied. The lattice is also used in the BSR, but re-matched to optimize the emittance and the beam parameters at the ports of beam lines. Fig. 2 shows the Twiss functions of the

Table 1. Main parameters of the BEPCⅡ rings.

	BER/BPR	BSR
beam energy/GeV	1.89	2.5
circumference/m	237.53	241.13
beam current/A	0.91	0.25
bunch current/mA/No.	9.8/93	⩽1/multi
natural bunch length/mm	13.6	12.0
RF frequency/MHz	499.8	499.8
harmonic number	396	402
emittance (x/y)/(nm·rad)	144/2.2	140
β function at IP (x/y)/m	1.0/0.015	10.0/10.0
crossing angle/mrad	±11	0
tune $(x/y/s)$	6.54/5.59/0.034	7.28/5.18/0.036
momentum compaction	0.024	0.016
energy spread	5.16×10^{-4}	6.67×10^{-4}
natural chromaticity (x/y)	$-10.8/-20.8$	$-9.0/-8.9$
luminosity/(cm^{-2}·s^{-1})	1×10^{33}	–

Received 6 January 2009
* Supported by National Natural Sciences Foundation of China (10725525)
1) E-mail: qinq@ihep.ac.cn

Table 2. Measured and design chromaticities.

nominal ξ_x/ξ_y	Meas. ξ_x/ξ_y	nominal ξ_x/ξ_y	Meas. ξ_x/ξ_y
$-5.0/-5.0$	$-5.33/-5.02$	$-1.0/-1.0$	$-1.28/-0.82$
$-3.0/-3.0$	$-3.19/-2.46$	$+1.0/+1.0$	$+1.05/+0.95$
$-2.0/-2.0$	$-2.33/-0.89$	$+5.0/+5.0$	$+4.50/+3.28$
natural ξ_{x0}/ξ_{y0}	$-11.7/-10.4$	Meas. ξ_{x0}/ξ_{y0}	$-10.3/-10.1$

BSR ring. In the following sections, we will discuss corrections of the beam optics, the beam parameters we got, single and multi-bunch beam phenomena, and the optimization of collision. At last, a summary will be given.

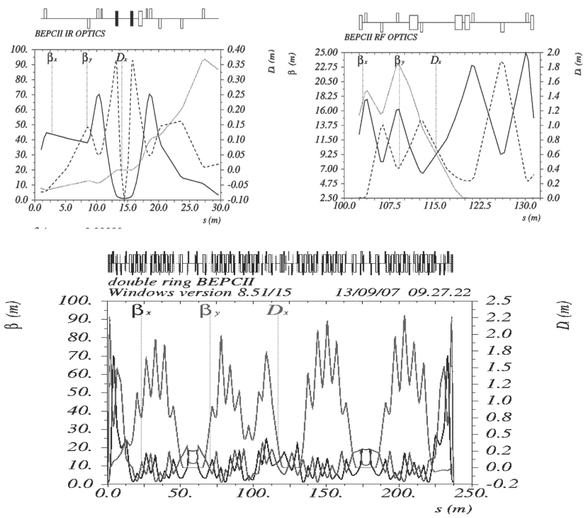

Fig. 1. Twiss functions in the IR (up-left), the RF region (up-right) and the whole ring (down) of BER/BPR.

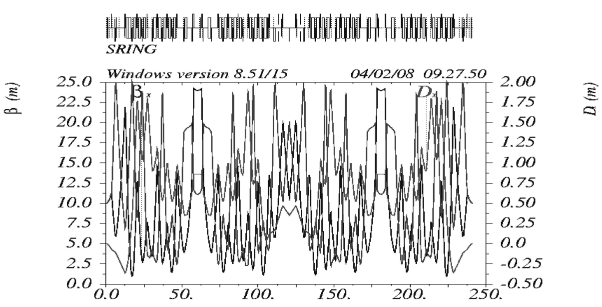

Fig. 2. Twiss functions of the BSR.

2 Determining beam parameters

2.1 Optics correction

After the beams were injected smoothly into the rings, the β functions along the rings were measured before and after the optics corrections based on the measured response matrices[2]. The code LOCO[3] was used to adjust the parameters of a computing model until the model response matrix fits the measured one well enough. The errors of quadrupole strength $\Delta K_{\rm q}$, BPM gain $\Delta G_{\rm i}$, corrector strength $\Delta\theta_{\rm j}$ and energy shift due to corrector $\Delta\delta_{\rm j}$, can be determined by the following expressions:

$$\chi^2=\sum_{\rm i,j}\frac{(M_{\rm mod,ij}-M_{\rm meas,ij})^2}{\sigma_{\rm i}^2}\equiv\sum_{\rm i,j}V_{\rm ij}^2 \qquad (1)$$

and

$$\Delta V_{\rm ij} = \sum\frac{\partial V_{\rm ij}}{\partial K_{\rm q}}\Delta K_{\rm q}+\sum\frac{\partial V_{\rm ij}}{\partial G_{\rm i}}\Delta G_{\rm i}+ \sum\frac{\partial V_{\rm ij}}{\partial \theta_{\rm j}}\Delta \theta_{\rm j}+\sum\frac{\partial V_{\rm ij}}{\partial \delta_{\rm j}}\Delta \delta_{\rm j}+\cdots, \qquad (2)$$

where $M_{\rm mod,ij}$ and $M_{\rm meas,ij}$ are the model and measured response matrices. Fig. 3 shows the measured response matrix with respect to the corrector strengths, and the readings of BPMs.

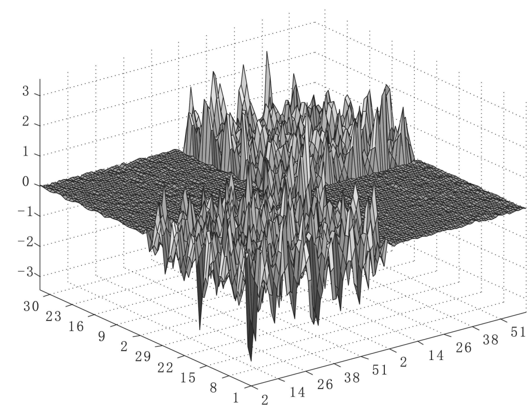

Fig. 3. Measured response matrix.

Figure 4 gives the distribution of residual differences between the measured and the fitted response matrices, normalized to the noise level of the individual BPMs. It means the fitting in LOCO converged to the noise level of BPMs.

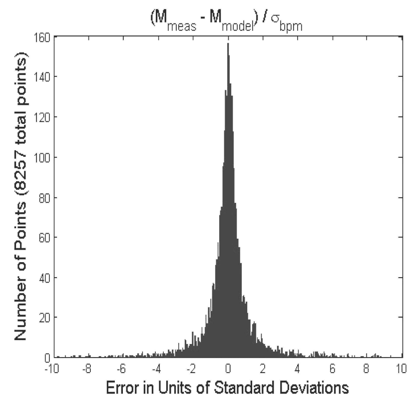

Fig. 4. Distribution of residual differences between the measured and fitted response matrices.

The beam optics was also analysed with the response matrix, and the quadrupole strengths were modified by the fudge factors defined as AF $= K/K_0$, or 1−AF, which could be calculated with LOCO. Almost all the big AFs were found to be related to hardware faults, such as short cut of magnet power supplies or grounding problems. Now most of the fudge factors of quadrupoles are less than 3%. The studies on the fringe field of bends and quads, and the interactions between quads and sextupoles in the arcs show that they are the main sources of the fudge factors. With the method of response matrix, we could correct the COD of the rings, generate the accurate local bumps, establish the slow orbit feedback system for the SR operation, compensate the wiggler effect in the SR operation and in the collision, and analyse any abrupt orbit change. Fig. 5 shows the BPM readings at the beam line ports before and after the slow orbit feedback system were applied. With this system, the vertical beam position shift could be controlled within ±10 μm.

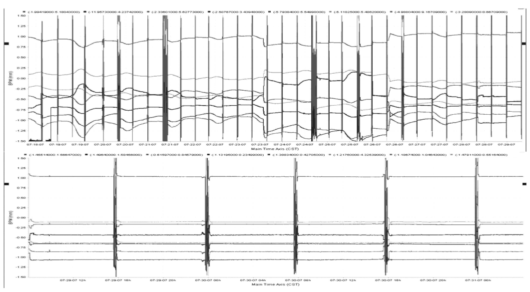

Fig. 5. BPMs' vertical readings at the beam line ports. (Upper and lower: before and after the SOFB applied).

2.2 Other beam parameters

After the beam optics correction, as shown in Fig. 6, the relative errors between the nominal and measured beta functions are less than 10% on the average. Other Twiss functions, such as dispersions and transverse tunes, were also measured and close to the design values. Under these circumstances, we could do some beam observations and measurements of other parameters.

The beta functions at the IP are measured with the same method, but the thick lens model is taken into account as we calculate the average beta at the edge of the first quad near the IP. Since the superconducting quads (SCQ) near the IP off-centrally bend the beam in horizontal, the contribution from this effect was also considered. The measured β_y^* of the both rings was ∼1.4 cm, which is very close to the design value.

The chromaticities of both rings were measured at the first stage of commissioning. Table 2 gives the measured and design chromaticities of the BSR.

The optimized RF frequency was also measured by measuring the transverse tunes at different chromaticities, shown as Fig. 7, which means the optimized RF frequency is very close to the design value.

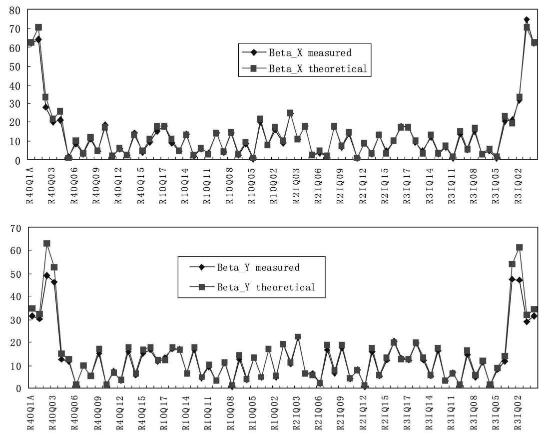

Fig. 6. Comparison between measured and nominal β functions in BER after optics correction.

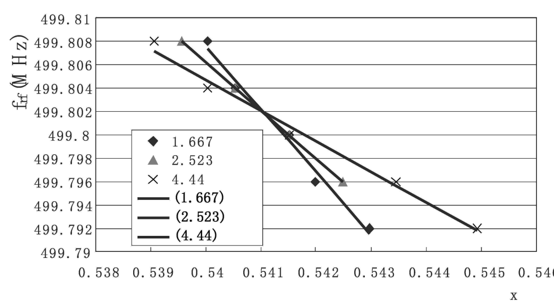

Fig. 7. Measurement of optimized RF frequency.

Transverse coupling was measured with the tune split method and could be adjusted by changing the vertical orbit in sextupoles. The coupling coefficient C_{12} was optimized by changing the transverse orbits.

Beam energy spread was got by measuring the longitudinal momentum acceptance. If the RF voltage is set to keep a relatively short beam lifetime, say 20 or 30 min, the longitudinal quantum lifetime can be considered as the dominant one. Thus, the beam energy spread at different bunch current could be estimated. Fig. 8 shows the beam energy spreads at different bunch current in both BER and BPR.

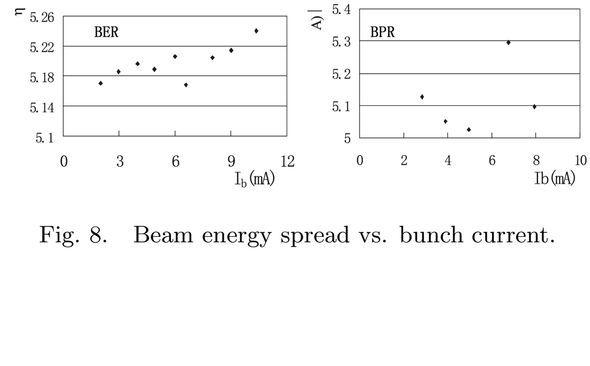

Fig. 8. Beam energy spread vs. bunch current.

The average beam energy spread of the two rings could be then got as 5.20×10^{-4} for BER and 5.12×10^{-4} for BPR.

3 Single beam dynamics

3.1 Bunch Lengthening

Bunch lengthening is one of the key issues to limit the luminosity in collider. Bunch lengthening in both BER and BPR was measured with a streak camera after the lattice correction. Single bunch was used for each beam without collision in the measurement. With the calibrated RF voltage and the measured synchrotron tune, the momentum compaction was calculated. The bunch length is fitted with the distribution of bi-Gaussian as that used in the previous BEPC[4]. Static image was measured and reduced from the measured bunch lengths. Fig. 9 shows the bunch lengthening as a function of bunch current in the BER and BPR, respectively.

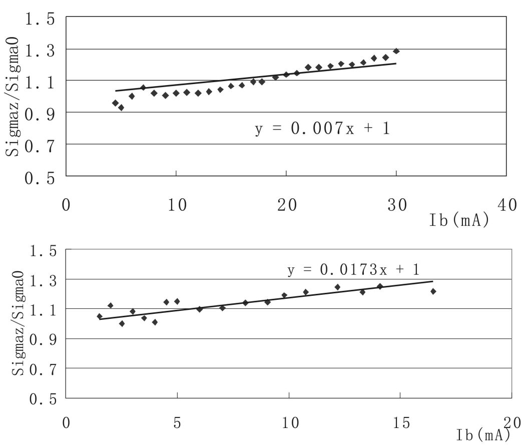

Fig. 9. Bunch lengthening vs. bunch current.

From the bunch lengthening, we can get the inductance of the BER and BPR as $L = 32.1$ nH and $L = 118$ nH, respectively, which correspond to $|Z/n|_0 = 0.25\ \Omega$ and $|Z/n|_0 = 0.94\ \Omega$. Since the bunch lengthens at low current due to potential well distortion, it can be expressed as[5]

$$\frac{\sigma_l}{\sigma_{l0}} \approx 1+\frac{e\alpha_p I_b \omega_0 L}{8\sqrt{\pi}\nu_s^2 E}\left(\frac{R}{\sigma_{l0}}\right)^3, \tag{3}$$

where σ_l and σ_{l0} are the bunch length at current I_b and the natural bunch length, respectively, α_p is the momentum compaction factor, ω_0 the angular revolutionary frequency, L the inductance, R the average radius of ring, ν_s the longitudinal tune, and E the beam energy. With the calculated L from the bunch lengthening measurement, we can get $\sigma_l/\sigma_{l0} \approx 0.0053I_b+1$ for the BER and $\sigma_l/\sigma_{l0} \approx 0.01855I_b+1$ for the BPR, respectively, which are similar to the fitting results shown in Fig. 9.

3.2 Tune variation

The effective impedance can also be estimated from the tune variation due to the changing of bunch current with the following expressions[6]:

$$\frac{d\nu_\perp}{dI} = \frac{R}{4\sqrt{\pi}(E/e)\sigma_l}\bar{\beta}_\perp Z_{\perp,\text{eff}}\ , \tag{4}$$

where $\bar{\beta}_\perp$ is the average β function around the ring. Fig. 10 shows the transverse tunes as functions of bunch current in both rings. All the measurements are done without beam collision, and the tunes are measured with FFT done by the signals taken from the single pass BPM. With Eq. (4) and $|Z/n|_0 = b^2 Z_{\perp,\text{eff}}/2R$, the estimated low frequency longitudinal impedances of the BER and BPR are $|Z/n|_0 = 1.29\ \Omega$ and $|Z/n|_0 = 1.10\ \Omega$, respectively. The errors of fitting are less than $\pm3\%$ after data filtering.

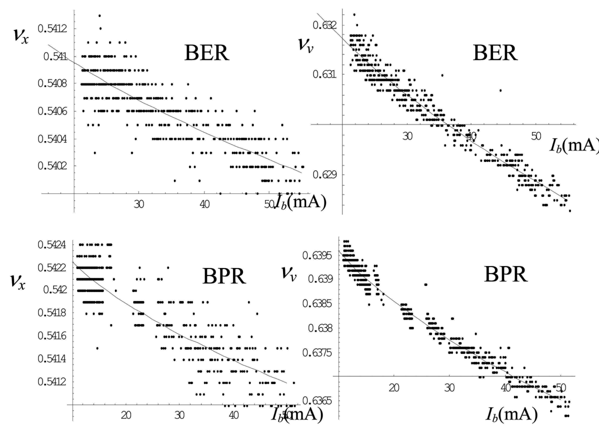

Fig. 10. Tune variation as a function of bunch current.

3.3 Single bunch beam lifetime

The single bunch beam lifetimes in the BER and BPR were measured for several times under different machine conditions, as shown in Fig. 11. The RF voltages are kept as 1.5 MV for enough longitudinal Touschek lifetime.

If we take the beam lifetime at low current as the Touschek lifetime, we can get 10 hrs@1 mA for both rings by extrapolating the curves in Fig. 11. It is far from the design Touschek lifetime of 7.1 hrs@9.8 mA. With the vacuum pressure given in the rings, the beam-gas lifetime can be estimated. The residual gas consists of about 70% CO and 30% H_2 in the BPR, and 30% CO and 70% H_2 in the BER. At the bunch current of 1 mA, the beam-gas lifetime of e+ beam is calculated as 146 hrs with the average vacuum pressure of 0.178 nTorr. So the total calculated lifetime of e+ beam is ∼43 hrs, which is larger than 10 hrs we observed and hints that the vacuum is not as good as expected in both rings.

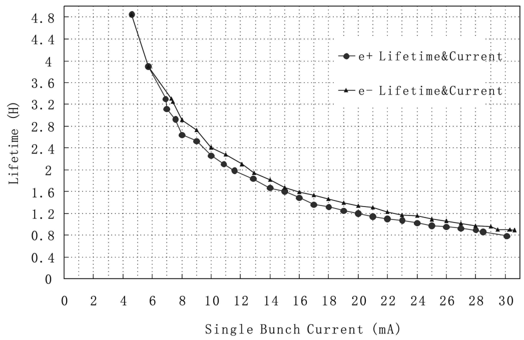

Fig. 11. Single bunch beam lifetime observation.

4 Multi-bunch beam dynamics

4.1 Multi-bunch beam lifetime

The beam lifetime of multi-bunch case is also observed with different beam currents and vacuum pressure. Fig. 12 depicts the average vacuum pressure under different beam current in both rings. Taking an example of 500 mA×500 mA in collision for both beams, we have the average vacuum pressure of 3.58 nTorr in BPR and 1.79 nTorr in BER. The various beam lifetimes calculated in both rings and the observed lifetimes are listed in Table 3.

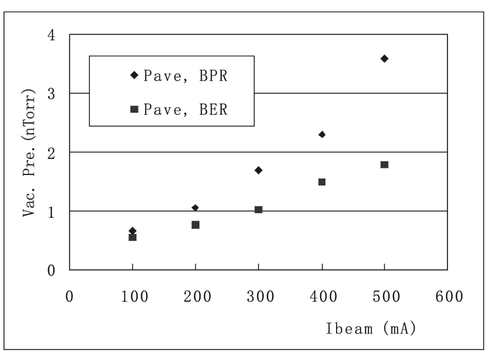

Fig. 12. Average vacuum at different beam current.

From Table 3, we can see that the e+ beam lifetime agrees very well with the observed one, while the e- beam doesn't. The reason should be the same as the single bunch case. It is believed that if the vacuum improved, the lifetime at very low bunch current should be longer, and the total beam lifetime would be longer too.

Table 3. Calculated and observed (obsd.) beam lifetime.

	⟨p⟩/ nTorr	b-g/ hr	Tous./ hr	b-b/ hr	total/ hr	obsd./ hr
BER	1.79	33	2.0	6.0	1.44	2.94
BPR	3.58	7.3	2.0	6.0	1.24	1.12

4.2 Electron cloud observations

The beam blow-up due to the electron cloud (EC) will cause the reduction of luminosity and the coupled bunch instability will limit the beam current. The electron cloud instability (ECI) was also observed clearly in the BPR, though the beam current is not very high. Fig. 13 shows the beam spectra in both rings. In Fig. 13, the beam current is 40 mA in both rings with the same filling pattern. We can easily find that there're more sidebands in BPR than those in BER, which is one of the main evidences of ECI.

Keeping the same filling pattern but changing the bunch current, we can find the threshold beam current of ECI for different bunch numbers, as the example shown in Fig. 14. Table 4 summarizes the threshold we got in the experiment. It seems the threshold current of ECI is low, which is about two times higher than that in BEPC[7]. The more detailed ECI observations, such as the mode distribution, and bunch size variation, can be found in Ref. [8].

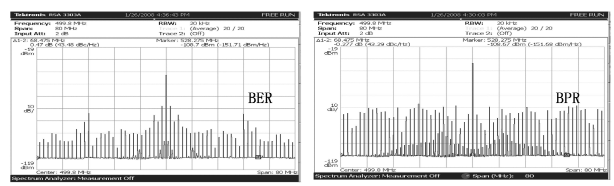

Fig. 13. Spectra of both rings with same $I_{\rm B}$.

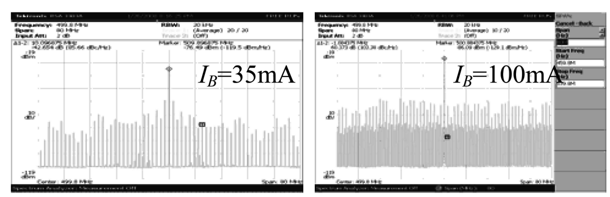

Fig. 14. Spectrum in BPR ($N_{\rm b}$=99, uniform filling).

Table 4. Threshold beam current of ECI.

$N_{\rm b}$	$S_{\rm b}$ (RF bucket)	$I_{\rm b}$/mA	$I_{\rm th}$/mA
48	8	∼1.0	∼50
99	4	∼0.35	∼35
198	2	∼0.15	∼30

5 Collision optimization

The collision with high luminosity is the final aim of the BEPCⅡ. The optimization of collision is based on the corrected beam optics and some other optimized beam parameters, such as transverse tunes, coupling, dynamic aperture, etc. A low background on the detector during beam injection and collision is also required for a better performance.

The beam-beam scan, as shown in Fig. 15, was done under the collision with single bunch per beam, with the finding of the transverse position offsets of two beams at the IP. The bunch sizes could also be fitted in the beam-beam scan.

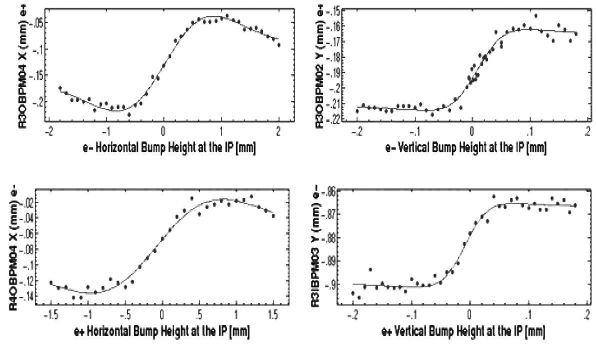

Fig. 15. A typical beam-beam scan for the transverse beam position offset at the IP. (upper: e-, lower: e+).

Optimizing transverse tune is one of the most important issues to get higher luminosity. The tune-luminosity scan of the BEPCⅡ shows that the peak luminosity happens at $\nu_x/\nu_y = 6.54/5.64$ of BER and $\nu_x/\nu_y = 6.545/5.636$ of BPR. At this tune range, we got the highest luminosity of $\geqslant 1\times10^{32}$ cm$^{-2}\cdot$s^{-1} with around 500 mA×500 mA for two colliding beams at the end of the 2$^{\text{nd}}$ commissioning stage.

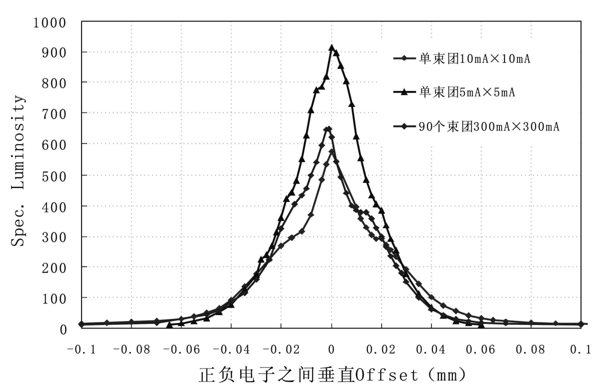

Fig. 16. Spec. Lum. vs. offsets between e+ and e- at different beam current.

The vertical offsets between two beams at the IP were measured to optimize the luminosity at different beam currents, shown as Fig. 16. The specific luminosity is defined as $L/(I^+\times I^-)$.

The beam lifetime was enlarged when two beams collided, which is thought to be the blow-up of the colliding bunches at the IP. Fig. 17 gives the beam lifetime and specific luminosity as functions of single bunch current. Transverse coupling was also optimized in both rings for a better luminosity.

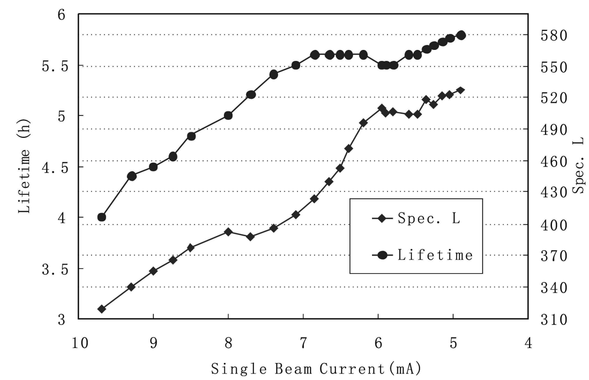

Fig. 17. Spec. Lum. and beam lifetime as functions of bunch current during collision.

6 Summary

The beam optics of the three rings of BEPCⅡ was corrected with the method of response matrix. Twiss functions were measured along the rings, and close to the nominal values. In addition, COD corrections, local bump generation, compensation of wiggler effect, and finding the faults of hardware, were also done with measured response matrices. Some current dependent phenomena were observed. Single bunch effects, such as bunch lengthening and tune variation revealed the impedance related issues, and the low frequency longitudinal impedances of the two rings were got. The measured Touschek beam lifetime was far from the calculated one, and thus the total beam lifetime did not agree well enough with the observed one. It could be explained somewhat that the vacuum was not as good as expected. ECI has been observed in the e+ ring of BEPCⅡ. The spectra and mode distribution were studied under different bunch patterns and currents. The threshold current of ECI with 99 uniform filling bunches was about 35 mA. Further studies on beam phenomena are needed. Beam collision was optimized by scanning the transverse offsets at IP, tune scan, coupling optimization, etc.

References

1 WANG J Q et al. Proc. Of PAC'07, June 2007
2 WEI Y Y. Proc. of PAC'07, June 2007
3 Safranek J. NIM A, 1997, **388**: 27
4 QIN Q et al. NIM A, 2001, **463**: 77—85
5 Zotter B. CERN 85-19, 1985
6 Heifets S A, Kheifets S A. Rev. Mod. Phys., 1991, **63**: 631
7 GUO Z Y et al. PRST-AB, 2002, **5**: 124403
8 LIU Y D et al. this proceedings